Rigid Molecular Rods with Cumulene-Bridged Polyphosphines: Synthesis, Electronic Communication, Molecular Photophysics, Mixed-Valence State, and X-ray Photoelectron Spectroscopic Study

Jeffrey V. Ortega, Bo Hong,* Sutapa Ghosal, and John C. Hemminger

Department of Chemistry, University of California, Irvine, California 92697-2025

Brian Breedlove and Clifford P. Kubiak

Department of Chemistry, University of California, San Diego, California 92093-0332

Received June 11, 1999

The synthesis, molecular photophysics, redox characteristics, and electronic interactions, as well as an X-ray photoelectron spectroscopic (XPS) study of a series of Ru(II) and Os(II) complexes with a polyphosphine/cumulene spacer, namely, 1,1′,4,4′-tetrakis(diphenylphosphino)cumulene (C_4P_4), are studied and compared with the corresponding systems containing spacers with shorter sp carbon chain (C_n) lengths. Characterizations of all mono-, homo-, and heterobimetallic complexes with PF_6^- counteranions are accomplished using ^1H, ^{13}C, and $^{31}P\{^1H\}$ NMR, fast atom bombardment (FAB/MS), and matrix-assisted laser desorption ionization time-of-flight (MALDI-TOF/MS) mass spectroscopy and elemental analysis. From the electrochemical study it is observed that the length of the C_n bridges has a profound influence on redox potentials and the electronic interaction between the two metal-based termini. XPS studies reveal that a simple change in carbon chain length affects the electron donation of the phosphine spacer to the metal-based termini. As a result, the redox potential of the Ru(II) or Os(II) center is shifted significantly. The comproportionation constant, K_c, is calculated as 1.3×10^7 ($M = Ru^{II}$) or 4.5×10^{10} ($M = Os^{II}$) for homobimetallic $[(bpy)_2M(C_4P_4)M(bpy)_2]^{4+}$, suggesting a strong electronic communication across the C_4P_4 spacer. However, the K_c value is estimated to be ca. 4 for the corresponding complexes $[(bpy)_2M(C_3P_4)M(bpy)_2]^{4+}$ (M = Ru, Os; C_3P_4 = 1,1′,3,3′-tetrakis(diphenylphosphino)allene), indicative of a system with electronic isolation between the two termini. In heterobimetallic $[(bpy)_2Ru(C_nP_4)Os(bpy)_2]^{4+}$ ($n = 3, 4$), the energy transfer from Ru(II) to Os(II) is found to be very efficient, with rate constants k_{en} of ca. 3×10^9 s^{-1} ($n = 3$) and 1×10^{11} s^{-1} ($n = 4$). The increased value of k_{en} upon the change from C_3 to C_4 can be explained by the increase in the electronic communication across spacers. Detailed studies and calculations have revealed a Dexter-type of mechanism for the triplet energy transfer in the system.

Introduction

The past decade has experienced rapidly growing interests in the areas of supramolecular photonic and electronic devices.[1] These devices require complex design and suitable assembly of active and/or passive components in space, time, and energetics, leading to the transportation of signal through intercomponent electron or energy transfer.[1,2] Such interests in supramolecular systems have stimulated the development of a variety of covalently linked multicomponent systems. These systems are based on metal-containing chromophores with emissive triplet excited states spanned by flexible or rigid spacers, which link between the photoactive donor/acceptor components or redox-active moieties.[2−6] A common objective in the construction of these low-dimensional supramolecular systems has been the rational assembly of individual components to achieve multicomponent devices that exhibit maximal electronic and excitonic interactions and, furthermore, the investigation and fine-tuning of parameters and factors that govern such interactions.[3−11] In addition, a judicious choice of spacer can be used to control the relative orientation and distance between the active components. As a result, the degree of electronic interaction, the efficiency and the rate constant of

* To whom the correspondence should be addressed.

(1) Lehn, J.-M. *Supramolecular Chemistry*: *Concepts and Perspectives*; VCH: Weinheim, Germany, 1995.

(2) Balzani, V.; Scandola, F. *Supramolecular Photochemistry*; Horwood: Chichester, U.K., 1991.

(3) (a) Sauvage, J.-P.; Colin, J.-P.; Chambron, J.-C.; Guillercz, S.; Cudret, C.; Balzani, V.; Barigelletti, F.; De Cola, L.; Flamigni, L. *Chem. Rev.* **1994**, *94*, 993. (b) Balzani, V.; Juris, A.; Venturi, M.; Campagna, S.; Serroni, S. *Chem. Rev.* **1996**, *96*, 759.

(4) (a) Brady, M.; Weng, W.; Zhou, Y.; Seyler, J. W.; Amoroso, A. J.; Arif, A. M.; Böhme, M.; Frenking, G.; Gladysz, J. A. *J. Am. Chem. Soc.* **1997**, *119*, 775. (b) Wärnmark, K.; Thomas, J. A.; Heyke, O.; Lehn, J.-M. *Chem. Commun.* **1996**, 701. (c) Meyer, T. J. *Pure Appl. Chem.* **1986**, *58*, 1193. (d) Wang, P.-W.; Fox, M. A. *Inorg. Chem.* **1995**, *34*, 36.

(5) (a) Ito, T.; Hamaguchi, T.; Nagino, H.; Yamaguchi, T.; Washington, J.; Kubiak, C. P. *Science* **1997**, *277*, 660. (b) Ito, T.; Hamaguchi, T.; Nagino, H.; Yamaguchi, T.; Kido, H.; Zavarine, I. S.; Richman, T.; Washington, J.; Kubiak, C. P. *J. Am. Chem. Soc.* **1999**, *121*, 4625. (c) Yang, J.; Seneviratne, D.; Arbatin, G.; Andersson, A. M.; Curtis, J. C. *J. Am. Chem. Soc.* **1997**, *119*, 5329.

(6) (a) Hong, B.; Ortega, J. V. *Angew. Chem., Int. Ed. Engl.* **1998**, *37*, 2131. (b) Hong, B.; Woodcock, S. R.; Saito, S. K. Ortega, J. V. *J. Chem. Soc., Dalton Trans.* **1998**, 2615. (c) Hong, B. *Comments Inorg. Chem.* **1998**, *20*, 177.

(7) (a) Harriman, A.; Ziessel, R. *Chem. Commun.* **1996**, 1707. (b) Grosshenny, V.; Harriman, A.; Ziessel, R. *Angew. Chem., Int. Ed. Engl.* **1995**, *34*, 1100. (c) Grosshenny, V.; Harriman, A.; Remero, F. M.; Ziessel, R. *J. Phys. Chem.* **1996**, *100*, 17472.

10.1021/ic990673m CCC: $18.00
Published on Web 10/09/1999

intercomponent (intramolecular) electron or energy transfer, and consequently the signal transition within supramolecular systems can be fine-tuned and controlled.

Representative spacers that have received extensive study in the past contained polypyridyl units (e.g., bipyridines or terpyridines).[3,7,9−11] In an effort to prepare new photoresponsive and redox-active supramolecular systems, we have used polyphosphines with rigid sp carbon chains as spacers. Specifically, allene-bridged 1,1′,3,3′-tetrakis(diphenylphosphino)allene (C_3P_4) and cumulene-bridged 1,1′,4,4′-tetrakis(diphenylphosphino)-cumulene (C_4P_4) have been explored together with the ligand 1,1′-bis(diphenylphosphino)ethene (C_2P_2e). C_2P_2e is used in the preparation of monometallic model complexes for photophysical and electrochemical studies. Using C_nP_4 ($n = 3, 4$) as coordination ligands and spacers, mono-, homo-, and heterobimetallic Ru(II)/Os(II) complexes can be prepared. Previously, we reported the preparation and molecular photophysics of complexes with C_2P_2e and C_3P_4,[6b] as well as the preliminary electrochemical study of complexes with C_n bridges ($n = 2-4$).[6a] Here we report an extensive study on the redox characteristics, electronic communication, molecular photophysics, mixed-valence state, and intramolecular energy transfer rate constants and mechanisms of complexes with C_4P_4, as well as the comparison with the corresponding complexes of C_3P_4 and C_2P_2e.

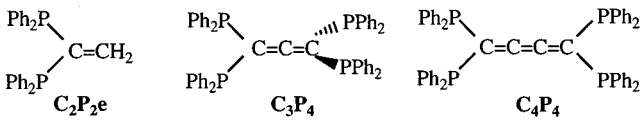

The advantage of using sp carbon chain spacers is that the unique structures of allene and cumulene bridges permit tuning of the electronic communication and the rate constant of energy or electron transfer across the spacer. The C_3 bridge will place the two termini at 90° relative to each other, while the C_4 bridge will maintain a coplanar structure of the two termini (Figure 1). As a result, the redox interaction and intramolecular electron/energy transfer rate constants can be readily controlled by changing the number of carbon atoms. Furthermore, we will report the first X-ray photoelectron spectroscopic study that describes the unusual electronic feature regarding how the simple change in the number of carbon atoms and the chain length in the spacer will affect the electron donation of the spacer to the metal-based termini. As a result, the redox potentials of both Ru(II) and Os(II) termini shift significantly. In addition to probing the electrochemical characteristics and molecular photophysics, investigation of the mixed-valence Ru/Os complexes has also been carried out to study the difference in electronic communication across spacers with different chain lengths (e.g., C_3 vs C_4).

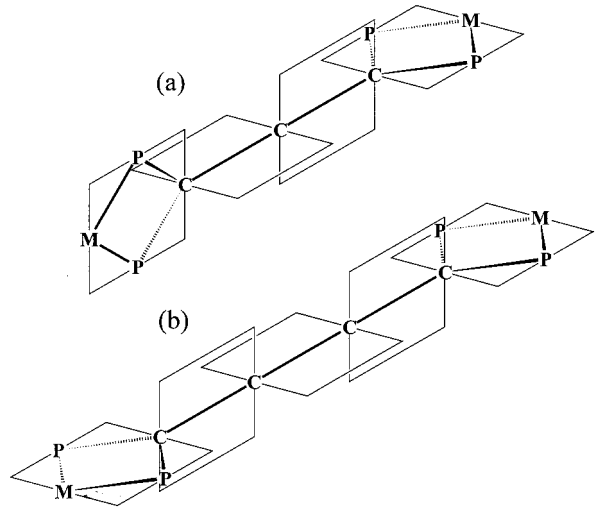

Figure 1. Representation of the π-orbital alignment of the allene-bridged bimetallic complexes (a) and that of the cumulene-bridged bimetallic complexes (b).

Experimental Section

General Methods. All experiments described below were performed under a nitrogen atmosphere using standard glovebox and Schlenk techniques. Separations by column chromatography were performed in air and in the absence of light using basic alumina (Brockman activity I, 60−325 mesh, from Fisher Scientific).

Materials. 1,1′,4,4′-Tetrakis(diphenylphosphino)cumulene (C_4P_4)[12] and *cis*-Os(bpy)$_2$Cl$_2$[8a,13] were prepared according to literature methods. *cis*-Ru(bpy)$_2$Cl$_2$ was purchased from Strem and used as received. Basic alumina and all Spectrograde solvents were purchased from Fisher and used without further purification. Tetrahydrofuran (THF), toluene, anhydrous diethyl ether, and hexanes were distilled under nitrogen from solutions containing sodium benzophenone ketyl. Acetonitrile (MeCN) was distilled under nitrogen over calcium hydride. Ethanol was distilled under nitrogen over magnesium. Ethylene glycol was dried over 4 Å molecular sieves for at least 24 h and deoxygenated by degassing with dry N_2 for 20 min or longer prior to use.

Physical Measurements. (a) NMR Study and Elemental Analysis. The $^{31}P\{^1H\}$ NMR spectra were obtained in acetonitrile-d_3 (MeCN-d_3) on an Omega 500 MHz spectrometer, referenced to a solution of 85% H_3PO_4 in D_2O. Combustion analyses (C, H, N) were obtained with a Carlo Erba Instruments Fisons elemental analyzer.

(b) Electrochemical Measurements. Cyclic voltammograms were recorded on a CHI 630 electrochemical analyzer. Typical experiments were run at 100 mV/s in acetonitrile with 0.1 M tetrabutylammonium hexafluorophosphate as electrolyte. A Ag/AgCl wire was used as the pseudoreference electrode, a platinum wire as the counterelectrode, and a 1.0 mm platinum disk electrode as the working electrode. A ferrocene standard was used to reference the observed potential vs SCE.

(c) FAB/MS and MALDI-TOF/MS Measurements. Fast atom bombardment mass spectra (FAB/MS) were recorded on a Fisons VG Autospec at the UCI mass spectral laboratory. Matrix-assisted laser desorption ionization time-of-flight mass spectra (MALDI-TOF/MS) were obtained on a PerSeptive Biosystems Voyager-DE Biospectrometry workstation equipped with a nitrogen laser (emission at 337 nm for 3 ns) and a linear detector. All measurements were done exclusively in the positive-ion mode. The matrix, dithranol, was dissolved in methylene chloride (10 mg/mL). Each sample solution (0.5 μL, ca.

(8) (a) Kober, E. M.; Caspar, J. V.; Sullivan, B. P.; Meyer, T. J. *Inorg. Chem.* **1988**, *27*, 4587. (b) Johnson, S. R.; Westmoreland, T. D.; Caspar, J. V.; Barqawi, K. R.; Meyer, T. J. *Inorg. Chem.* **1988**, *27*, 3195. (c) Kober, E. M.; Sullivan, B. P.; Dressick, W. J.; Caspar, J. V.; Meyer, T. J. *J. Am. Chem. Soc.* **1980**, *102*, 7383.

(9) (a) Richardson, D. E.; Taube, H. *Inorg. Chem.* **1981**, *20*, 1278. (b) Richardson, D. E.; Taube, H. *Coord. Chem. Rev.* **1984**, *60*, 107. (c) Salaymeh, F.; Berhane, S.; Yusof, R.; de la Rosa, R.; Fung, E. Y.; Matamoros, R.; Lau, K. W.; Zheng, Q.; Kober, E. M.; Curtis, J. C. *Inorg. Chem.* **1993**, *32*, 3895. (d) Coat, F.; Lapinte, C. *Organometallics* **1996**, *15*, 477. (e) Narvor, N. L.; Toupet, L.; Lapinte, C. *J. Am. Chem. Soc.* **1995**, *117*, 7129. (f) Patoux, C.; Launay, J.-P.; Beley, M.; Chodorowski-Kimmes, S.; Collin, J.-P.; James, S.; Sauvage, J.-P. *J. Am. Chem. Soc.* **1998**, *120*, 3717.

(10) Robin, M. B.; Day, P. *Adv. Inorg. Chem. Radiochem.* **1967**, *10*, 247.

(11) (a) Richter, M. M.; Brewer, K. J. *Inorg. Chem.* **1993**, *32*, 2827. (b) Benniston, A. C.; Goulle, V.; Harriman, A.; Lehn, J.-M. *J. Phys. Chem.* **1994**, *98*, 7798.

(12) (a) Schmidbaur, H.; Pollok, T. *Angew. Chem., Int. Ed. Engl.* **1986**, *25*, 348. (b) Schmidbaur, H.; Manhart, S.; Schier, A. *Chem. Ber.* **1993**, *126*, 2389.

(13) Buckingham, D. A.; Dwyer, F. P.; Goodwin, H. A.; Sargeson, A. M. *Aust. J. Chem.* **1964**, *17*, 325.

Table 1. Comparison of FAB/MS and MALDI-TOF/MS Data

complex	FAB, *m/z* [rel %]	FAB assignment	MALDI, *m/z* [rel %]	MALDI assignment
RuC_4P_4	1512 [10]	$[(bpy)_2Ru(C_4P_4)](PF_6)_2^+ + O$	1365 [6]	$[(bpy)_2Ru(C_4P_4)](PF_6)^+ + O$
	1496 [15]	$[(bpy)_2Ru(C_4P_4)](PF_6)_2^+$	1348 [11]	$[(bpy)_2Ru(C_4P_4)](PF_6)^+$
	1381 [100]	$[(bpy)_2Ru(C_4P_4)](PF_6)^+ + 2O$	1324 [12]	$[(bpy)_2Ru(C_4P_4)]^+ + O$
	1365 [30]	$[(bpy)_2Ru(C_4P_4)](PF_6)^+ + O$	1307 [11]	$[(bpy)_2Ru(C_4P_4)]^+$
	1349 [45]	$[(bpy)_2Ru(C_4P_4)](PF_6)^+$	1270 [31]	$[(bpy)_2Ru(C_4P_4)]^+ + 2O + 2F$
			1254 [37]	$[(bpy)_2Ru(C_4P_4)]^+ + O + 2F$
			1238 [27]	$[(bpy)_2Ru(C_4P_4)]^+ + 2F$
			1180 [17]	$[(bpy)_2Ru(C_4P_4)](PF_6)^+ - PPh_2 + O$
			1165 [18]	$[(bpy)_2Ru(C_4P_4)](PF_6)^+ - PPh_2$
			1146 [17]	$[(bpy)_2Ru(C_4P_4)](PF_6)^+ - PPh_2 - F$
			1069 [100]	$[(bpy)_2Ru(C_4P_4)]^+ - PPh_2 + 3O$
OsC_4P_4	1618 [100]	$[(bpy)_2Os(C_4P_4)](PF_6)_2^+ + 2O$	1584 [15]	$[(bpy)_2Os(C_4P_4)](PF_6)_2^+$
	1601 [55]	$[(bpy)_2Os(C_4P_4)](PF_6)_2^+ + O$	1488 [16]	$[(bpy)_2Os(C_4P_4)](PF_6)^+ + 3O$
	1585 [75]	$[(bpy)_2Os(C_4P_4)](PF_6)_2^+$	1472 [33]	$[(bpy)_2Os(C_4P_4)](PF_6)^+ + 2O$
	1526 [20]	$[(bpy)_2Os(C_4P_4)](PF_6)^+ + 3F + 2O$	1454 [11]	$[(bpy)_2Os(C_4P_4)](PF_6)^+ + O$
	1510 [35]	$[(bpy)_2Os(C_4P_4)](PF_6)^+ + 3F + O$	1341 [52]	$[(bpy)_2Os(C_4P_4)]^+ + 3O$
	1494 [45]	$[(bpy)_2Os(C_4P_4)](PF_6)^+ + 3F$	1327 [100]	$[(bpy)_2Os(C_4P_4)]^+ + 2O$
	1471 [55]	$[(bpy)_2Os(C_4P_4)](PF_6)^+ + 2O$		
	1455 [75]	$[(bpy)_2Os(C_4P_4)](PF_6)^+ + O$		
	1437 [15]	$[(bpy)_2Os(C_4P_4)](PF_6)^+$		
RuC_4P_4Ru	2031 [10]	$[(bpy)_2Ru(C_4P_4)Ru(bpy)_2](PF_6)_3^+ - F$	2124 [10]	$[(bpy)_2Ru(C_4P_4)Ru(bpy)_2](PF_6)_4^+ - 4F$
	1936 [45]	$[(bpy)_2Ru(C_4P_4)Ru(bpy)_2](PF_6)_2^+ + 2O$	1792 [7]	$[(bpy)_2Ru(C_4P_4)Ru(bpy)_2](PF_6)^+ + 2O$
	1920 [20]	$[(bpy)_2Ru(C_4P_4)Ru(bpy)_2](PF_6)_2^+ + O$	1778 [7]	$[(bpy)_2Ru(C_4P_4)Ru(bpy)_2](PF_6)^+ + O$
	1904 [10]	$[(bpy)_2Ru(C_4P_4)Ru(bpy)_2](PF_6)_2^+$	1762 [7]	$[(bpy)_2Ru(C_4P_4)Ru(bpy)_2](PF_6)^+$
	1881 [20]	$[(bpy)_2Ru(C_4P_4)Ru(bpy)_2](PF_6)_3^+ - PPh_2 + O$	1719 [9]	$[(bpy)_2Ru(C_4P_4)Ru(bpy)_2](PF_6)_2^+ - PPh_2$
			1665 [11]	$[(bpy)_2Ru(C_4P_4)Ru(bpy)_2]^+ + 3O$
	1818 [30]	$[(bpy)_2Ru(C_4P_4)Ru(bpy)_2](PF_6)^+ + 3F$	1649 [14]	$[(bpy)_2Ru(C_4P_4)Ru(bpy)_2]^+ + 2O$
	1775 [20]	$[(bpy)_2Ru(C_4P_4)Ru(bpy)_2](PF_6)^+ + O$	1634 [15]	$[(bpy)_2Ru(C_4P_4)Ru(bpy)_2]^+ + O$
	1759 [30]	$[(bpy)_2Ru(C_4P_4)Ru(bpy)_2](PF_6)^+$	1616 [12]	$[(bpy)_2Ru(C_4P_4)Ru(bpy)_2]^+$
	1630 [35]	$[(bpy)_2Ru(C_4P_4)Ru(bpy)_2]^+ + O$	1595 [17]	$[(bpy)_2Ru(C_4P_4)Ru(bpy)_2](PF_6)^+ - PPh_2 + F$
	1614 [25]	$[(bpy)_2Ru(C_4P_4)Ru(bpy)_2]^+$	1577 [13]	$[(bpy)_2Ru(C_4P_4)Ru(bpy)_2](PF_6)^+ - PPh_2$
	1574 [40]	$[(bpy)_2Ru(C_4P_4)Ru(bpy)_2](PF_6)^+ - PPh_2$	1400 [30]	$[(bpy)_2Ru(C_4P_4)Ru(bpy)_2]^+ - PPh_2 + 3O - 4F$
			1383 [61]	$[(bpy)_2Ru(C_4P_4)Ru(bpy)_2]^+ - PPh_2 + 2O - 4F$
	1552 [55]	$[(bpy)_2Ru(C_4P_4)Ru(bpy)_2](PF_6)^+ - PPh_2 - F$	1475 [27]	$[(bpy)_2Ru(C_4P_4)Ru(bpy)_2]^+ - PPh_2 + 3O$
			1459 [49]	$[(bpy)_2Ru(C_4P_4)Ru(bpy)_2]^+ - PPh_2 + 2O$
	1427 [100]	$[(bpy)_2Ru(C_4P_4)Ru(bpy)_2]^+ - PPh_2$	1271 [59]	$[(bpy)_2Ru(C_4P_4)Ru(bpy)_2]^+ - 2PPh_2 + 2O$
			1257 [76]	$[(bpy)_2Ru(C_4P_4)Ru(bpy)_2]^+ - 2PPh_2 + O$
			1242 [100]	$[(bpy)_2Ru(C_4P_4)Ru(bpy)_2]^+ - 2PPh_2$
OsC_4P_4Os	2101 [15]	$[(bpy)_2Os(C_4P_4)Os(bpy)_2](PF_6)_2^+ + O$	2086 [40]	$[(bpy)_2Os(C_4P_4)Os(bpy)_2](PF_6)_2^+$
	1997 [75]	$[(bpy)_2Os(C_4P_4)Os(bpy)_2](PF_6)^+ + 3F$	2040 [40]	$[(bpy)_2Os(C_4P_4)Os(bpy)_2](PF_6)_3^+ - PPh_2$
	1953 [10]	$[(bpy)_2Os(C_4P_4)Os(bpy)_2](PF_6)^+ + O$	1998 [100]	$[(bpy)_2Os(C_4P_4)Os(bpy)_2](PF_6)^+ + 3F$
	1937 [40]	$[(bpy)_2Os(C_4P_4)Os(bpy)_2](PF_6)^+$	1939 [60]	$[(bpy)_2Os(C_4P_4)Os(bpy)_2](PF_6)^+$
	1914 [35]	$[(bpy)_2Os(C_4P_4)Os(bpy)_2](PF_6)_2^+ - PPh_2 + O$	1852 [56]	$[(bpy)_2Os(C_4P_4)Os(bpy)_2]^+ + 4O$
			1836 [32]	$[(bpy)_2Os(C_4P_4)Os(bpy)_2]^+ + 3O$
	1898 [35]	$[(bpy)_2Os(C_4P_4)Os(bpy)_2](PF_6)_2^+ - PPh_2$	1823 [48]	$[(bpy)_2Os(C_4P_4)Os(bpy)_2]^+ + 2O$
			1808 [80]	$[(bpy)_2Os(C_4P_4)Os(bpy)_2]^+ + O$
	1856 [100]	$[(bpy)_2Os(C_4P_4)Os(bpy)_2]^+ + 4O$	1793 [32]	$[(bpy)_2Os(C_4P_4)Os(bpy)_2]^+$
RuC_4P_4Os	2139 [10]	$[(bpy)_2Os(C_4P_4)Ru(bpy)_2](PF_6)_3^+$	2156 [35]	$[(bpy)_2Os(C_4P_4)Ru(bpy)_2](PF_6)_3^+ + O$
	1997 [65]	$[(bpy)_2Os(C_4P_4)Ru(bpy)_2](PF_6)_2^+$	2114 [31]	$[(bpy)_2Os(C_4P_4)Ru(bpy)_2](PF_6)_4^+ - PPh_2 + O$
	1937 [100]	$[(bpy)_2Os(C_4P_4)Ru(bpy)_2](PF_6)_3^+ - PPh_2 - F$	2098 [27]	$[(bpy)_2Os(C_4P_4)Ru(bpy)_2](PF_6)_4^+ - PPh_2$
			1999 [39]	$[(bpy)_2Os(C_4P_4)Ru(bpy)_2](PF_6)_2^+$
	1850 [5]	$[(bpy)_2Os(C_4P_4)Ru(bpy)_2](PF_6)^+$	1958 [42]	$[(bpy)_2Os(C_4P_4)Ru(bpy)_2](PF_6)_3^+ - PPh_2$
			1939 [54]	$[(bpy)_2Os(C_4P_4)Ru(bpy)_2](PF_6)_3^+ - PPh_2 - F$
			1853 [96]	$[(bpy)_2Os(C_4P_4)Ru(bpy)_2](PF_6)^+$
			1811 [92]	$[(bpy)_2Os(C_4P_4)Ru(bpy)_2](PF_6)_2^+ - PPh_2$
			1795 [100]	$[(bpy)_2Os(C_4P_4)Ru(bpy)_2](PF_6)_2^+ - PPh_2 - F$
			1706 [35]	$[(bpy)_2Os(C_4P_4)Ru(bpy)_2]^+$

$10^{-4}-10^{-5}$ M) was applied to a gold-plated sample holder and allowed to dry. Then 0.5 μL of the dithranol solution was applied and dried in air. FAB/MS and MALDI-TOF/MS data are included in Table 1.

(d) Photophysical Measurements. Absorbance spectra were recorded on a Hewlett-Packard 8453 diode array spectrophotometer. Steady-state emission spectra were obtained on a Hitachi F-4500 fluorescence spectrometer. Luminescence quantum yields of all complexes were measured in Spectrograde acetonitrile relative to $Ru(bpy)_3(PF_6)_2$ ($\Phi = 0.062$[14] in acetonitrile).

The time-resolved emission spectroscopic study was carried out on a nanosecond laser flash photolysis unit equipped with a Continuum Surelite II-10 Q-switched Nd:YAG laser and Surelite OPO (optical parametric oscillator) tunable visible source, a LeCroy 9350A oscilloscope, and a Spex 270 MIT-2x-FIX high-performance scanning and imaging spectrometer.

(e) XPS Analysis. X-ray photoelectron spectroscopy (XPS) was carried out using an ESCALAB MKII (a multitechnique surface analysis instrument based on a UHV system) photoelectron spectrometer (VG Scientific). Typical background pressures were $(7-20) \times 10^{-10}$ Torr. All experiments were carried out with a standard Mg/Al twin anode

(14) (a) Caspar, J. V.; Meyer, T. J. *J. Am. Chem. Soc.* **1983**, *105*, 5583. (b) Caspar, J. V.; Sullivan, B. P.; Meyer, T. J. *Inorg. Chem.* **1984**, *23*, 2104.

X-ray source and a 150 mm radius hemispherical electron energy analyzer. Mg Kα X-rays (1253.6 eV) were used in the experiments described here. All spectra were obtained using constant analyzer pass energy (pass energy of 20 eV for the narrow scans and 50 eV for the survey scans). Powder samples were used in the XPS experiments. Samples were prepared by pressing the powder onto the surface of stainless steel sample holders that had been precoated with a polymer-based double-sided adhesive tape. The samples were left overnight in a vacuum desiccator before introducing them into the UHV chamber. They were then vacuum-pumped for a couple of hours under UHV conditions before the actual measurements.

(f) Chemical Oxidation with Ce(IV) and Spectroelectrochemical Near-IR Study. The Os(II) complexes were oxidized chemically in an acetonitrile−water (10:1 v/v) mixture. The solutions of the Os(II) homo- and bimetallic complexes (1×10^{-4} M) were titrated with microliter aliquots of a 5.5×10^{-3} M Ce(IV) solution. The titration was performed by monitoring the change in absorbance in the visible region where the Os(II) species exhibit intense absorption bands, whereas the absorbance of the Os(III) species is very small.[11c,d] The near-IR study of the resulting mixed-valence complexes was carried out on a Bruker IFS-66 FT-IR spectrometer.

The reflectance near-IR spectroelectrochemistry (NIR SEC) experiments were performed as described elsewhere.[5a,b] An EG&G PAR model 363 potentiostat and a Shimadzu UV-3101PC UV−vis−NIR scanning spectrometer were used to affect and monitor thin-layer bulk electrolysis, respectively. The RuC_4P_4Os complex was placed in an acetonitrile solution containing 0.1 M tetra-*n*-butylammonium hexafluorophosphate. The concentration of RuC_4P_4Os used for this measurement was 2.0 mM. Once the sample solution was degassed with N_2, the mixture was placed in the SEC cell, which has been described before.[5a,b] A background measurement was then performed with no applied voltage, which was subsequently subtracted from all future measurements. A near-IR measurement was then made with an applied voltage of 1.215 V, where only the Os(II) center was oxidized to Os(III).

$[(bpy)_2M(C_4P_4)](PF_6)_2$ (M = Ru, RuC_4P_4; M = Os, OsC_4P_4). A solution of $(bpy)_2MCl_2$ (M = Ru, Os) (1.0 equiv) in ethylene glycol (20 mL) was added dropwise to a refluxing solution of C_4P_4 (2 equiv) in THF (60 mL). The resulting mixture was refluxed for 15 h. An excess amount of NH_4PF_6 (ca. 10 equiv) was then added, and the mixture was refluxed for an additional 60 h to ensure the completion of the reaction. The solution was cooled to room temperature, and the THF portion of the reaction mixture was removed by rotary evaporation. The resulting ethylene glycol solution was added dropwise to a saturated solution of KPF_6 in H_2O (200 mL). The precipitate was collected by vacuum filtration, washed with H_2O (3×20 mL) and diethyl ether (3×20 mL), and dried in vacuo. The product was purified by column chromatography as the first fraction, using basic alumina and an acetonitrile/toluene (60:40 v/v) eluent.

RuC_4P_4. Yield: 48%. $^{31}P\{^1H\}$ NMR (202 MHz, MeCN-d_3): δ 13.91, 5.95 ppm. Anal. Calc for $C_{72}H_{56}N_4F_{12}P_6Ru$: C, 57.95; N, 3.75; H, 3.78. Found: C, 57.75; N, 3.78; H, 3.76.

OsC_4P_4. Yield: 56%. $^{31}P\{^1H\}$ NMR (MeCN-d_3): δ −26.99, −30.74 ppm. Anal. Calc for $C_{72}H_{56}N_4F_{12}P_6Os$: C, 54.69; N, 3.54; H, 3.57. Found: C, 54.74; N, 3.85; H, 3.91.

$[(bpy)_2M(C_4P_4)M(bpy)_2](PF_6)_4$ (M = Ru, RuC_4P_4Ru; M = Os, OsC_4P_4Os). A hot solution of C_4P_4 (1.0 equiv) in THF (40 mL) was added dropwise to a heated solution of $(bpy)_2MCl_2$ (M = Ru, Os) (2.2 equiv) in ethylene glycol (20 mL) at 120 °C. The resulting mixture was refluxed for 15 h and then allowed to cool to room temperature. An excess amount of NH_4PF_6 (ca. 10 equiv) was added, and the mixture was refluxed for an additional 60 h. The mixture was again cooled to room temperature, and the THF portion of the solvent mixture was removed by rotary evaporation. The resulting ethylene glycol solution was added slowly to a saturated solution of KPF_6 in H_2O (200 mL). The precipitate was collected by vacuum filtration, washed with H_2O (3×20 mL) and diethyl ether (3×20 mL), and dried in vacuo. The homobimetallic product was isolated as the second fraction, using basic alumina and an acetonitrile/toluene (60:40 v/v) solvent mixture.

RuC_4P_4Ru. Yield: 57%. $^{31}P\{^1H\}$ NMR (MeCN-d_3): δ −2.24 ppm. Anal. Calc for $C_{92}H_{72}N_8F_{24}P_8Ru_2$: C, 50.33; N, 5.10; H, 3.30. Found: C, 50.56; N, 5.25; H, 3.26.

OsC_4P_4Os. Yield: 27%. $^{31}P\{^1H\}$ NMR (MeCN-d_3): δ −5.11 ppm. Anal. Calc for $C_{92}H_{72}N_8F_{24}P_8Os_2$: C, 46.55; N, 4.72; H, 3.05. Found: C, 46.70; N, 4.92; H, 3.01.

$[(bpy)_2Os(C_4P_4)Ru(bpy)_2](PF_6)_4$ (RuC_4P_4Os). A solution of OsC_4P_4 (75 mg, 0.047 mmol) in MeCN (20 mL) was added to a heated solution of $(bpy)_2RuCl_2$ (24.7 mg, 0.047 mmol) in ethylene glycol (15 mL) at 110 °C. The mixture was refluxed for 15 h and cooled to room temperature, and an excess amount of NH_4PF_6 (ca. 10 equiv) was added. The reaction mixture was refluxed for an additional 60 h. The mixture was again cooled to room temperature, and the THF portion of the solvent mixture was removed by rotary evaporation. The resulting ethylene glycol solution was added dropwise to a saturated solution of KPF_6 in H_2O (200 mL). The precipitate was collected by vacuum filtration, washed with H_2O (3×20 mL) and diethyl ether (3×20 mL), and dried in vacuo. The purified product was obtained as the second portion using basic alumina and an acetonitrile/toluene (60:40 v/v) eluent. Yield: 43.5 mg (42%). $^{31}P\{^1H\}$ NMR (MeCN-d_3): δ 83.54, −5.89 ppm. Anal. Calc for $C_{92}H_{72}N_8F_{24}P_8RuOs$: C, 48.36; N, 4.90; H, 3.17. Found: C, 48.38; N, 4.99; H, 3.23.

Results and Discussion

Synthetic Aspects. The spacer C_4P_4 was prepared from the ditopic ligand $Ph_2PC{\equiv}CPPh_2$ using procedures initially reported by Schmidbaur and co-workers.[12] Suitable monomeric precursors, namely, $M(bpy)_2Cl_2$ (M = Ru, Os), were used to react with this spacer. Different metal-to-spacer ratios were used in order to obtain a monometallic (metal-to-spacer ratio 1:2) or homobimetallic (metal-to-spacer ratio 2.2:1) complex as the predominant product. The pure complex was obtained after column chromatographic separation using basic alumina. For the heterobimetallic complex RuC_4P_4Os, a reaction between OsC_4P_4 and $Ru(bpy)_2Cl_2$ in an ethylene glycol and acetonitrile mixture was employed, followed by purification with chromatographic separation.

FAB/MS and MALDI-TOF/MS Studies. Upon purification, structural identification of all new complexes was carried out using both FAB/MS and MALDI-TOF/MS analysis. Representative data for each compound are included in Table 1.

Several representative features are observed in both FAB/MS and MALDI-TOF/MS studies. (i) All fragments correspond to species with a +1 charge. This was also observed for the series of complexes with Ru(II)/Os(II) centers and a C_3P_4 ligand.[6b] (ii) Although the fragments observed in the FAB/MS and MALDI-TOF/MS analyses for each compound are different, loss of PF_6, PPh_2, and F units has been observed for all complexes. (iii) The addition of one, two, or even three O atoms is found in fragments using both types of mass spectral analysis although all complexes are stable in air. No additional peaks are found in $^{31}P\{^1H\}$ NMR spectra which correspond to the oxidized species. (iv) The inner-sphere metal−phosphine coordination is left intact, making peak identification straightforward.

Redox Potential and Electronic Interaction. The metal-based oxidations and ligand-based reductions in the cyclic voltammetry study of all compounds with C_4P_4 are listed in Table 2. When we inspect the redox potentials of the monomeric Ru^{II} or Os^{II} complexes with C_4P_4 and compare them with those of complexes containing C_2P_2e or C_3P_4, several interesting features arise regarding the redox potentials and their shift as a function of carbon chain length, as well as the electronic interaction across rigid spacers.

For monomeric complexes, it was observed that the number of carbon atoms and the carbon chain length have a profound influence on the metal-based oxidations. The redox potentials

Table 2. Formal Potentials (vs SCE) for Ru^{II} and Os^{II} Complexes with C_4P_4

complex	$Ru^{II/III}$ $E_{1/2}$, V (ΔE_p, mV)	$Os^{II/III}$ $E_{1/2}$, V (ΔE_p, mV)	1st $bpy^{0/-}$ $E_{1/2}$, V (ΔE_p, mV)	2nd $bpy^{0/-}$ $E_{1/2}$, V (ΔE_p, mV)
RuC_4P_4	+1.07 (1e⁻, 82)		−1.42 (1e⁻, 79)	−1.67 (1e⁻, 109)
OsC_4P_4		+0.80 (1e⁻, 62)	−1.32 (1e⁻, 71)	−1.56 (1e⁻, 102)
RuC_4P_4Ru	+1.01 (1e⁻, 69) +1.43 (1e⁻, 63)		−1.19 (2e⁻, 73)	−1.34 (2e⁻, 106)
OsC_4P_4Os		+0.72 (1e⁻, 78) +1.35 (1e⁻, 76)	−1.36 (2e⁻, 44)	−1.69 (2e⁻, 104)
RuC_4P_4Os	+1.32 (1e⁻, 78)	+0.74 (1e⁻, 78)	−1.28 (2e⁻, 94)	−1.45 (2e⁻, 93)

of the $M^{II/III}$ (M = Ru, Os) couples in MC_4P_4 (M = Ru, $E_{1/2}$ = +1.07 V; M = Os, $E_{1/2}$ = +0.80 V vs SCE) are much lower than those of MC_2P_2e (M = Ru, $E_{1/2}$ = +1.70 V; M = Os, $E_{1/2}$ = +1.35 V vs SCE) or MC_3P_4 (M = Ru, $E_{1/2}$ = +1.55 V; M = Os, $E_{1/2}$ = +1.12 V vs SCE).[6a,b] In other words, as the carbon chain length increases, the metal-based oxidation decreases significantly. We will discuss this trend in more detail together with the X-ray photoelectron spectroscopic study later.

For the homobimetallic complexes MC_4P_4M, two consecutive reversible one-electron oxidations (eq 1) are observed, with $E_1°$

$$M^{II}(C_4P_4)M^{II} \underset{E_1°}{\overset{e^-}{\rightleftharpoons}} M^{II}(C_4P_4)M^{III} \underset{E_2°}{\overset{e^-}{\rightleftharpoons}} M^{III}(C_4P_4)M^{III} \quad (1)$$

= +1.01 V and $E_2°$ = +1.43 V for the Ru complex and $E_1°$ = +0.72 V and $E_2°$ = +1.35 V for the Os^{II} complex. In comparison with the case for the corresponding monomeric complexes with C_4P_4, the first oxidation of MC_4P_4 M occurs at a less positive potential and the second one occurs at a much higher potential. The relatively large separations between the redox potentials of the two metal centers ($\Delta E_{1/2}$ = 630 mV for OsC_4P_4Os and 420 mV for RuC_4P_4Ru) are ascribed to a strong electronic communication between the two terminal subunits spanned by C_4P_4.[9] In contrast, the homobimetallic complexes MC_3P_4M with allene bridges exhibit two overlapping one-electron processes at +1.07 V (M = Ru) and +0.77 V (M = Os), eq 2.[6b] The cyclic voltammograms of RuC_3P_4Ru

$$M^{II}(C_3P_4)M^{II} \overset{2e^-}{\rightleftharpoons} M^{III}(C_3P_4)M^{III} \quad (2)$$

and RuC_4P_4Ru are compared in Figure 2. The overlapping of the two $M^{II/III}$ redox couples of RuC_3P_4Ru corresponds to the situation where the two termini are in electronic isolation. Hence, with the change of one carbon atom in the sp carbon chain unit, the redox interaction across the spacer has been dramatically modified. The difference here can be ascribed to the fact that an odd number of carbons (C_3) will cause the two metal-based termini to lie at 90° to each other (Figure 1a), while the one with a cumulene (C_4) bridge will place the two termini on the same plane (Figure 1b). The former will cause electronic isolation between the termini, but the latter will afford conjugation that facilitates the electronic interaction.

For MC_4P_4M (M = Ru, Os) complexes that undergo multistep charge transfer (eq 1), the equilibrium constant (K_c) for the comproportionation reaction is defined as shown in eq 3, with

$$K_c = \frac{[M^{II}(C_4P_4)M^{III}]^2}{[M^{II}(C_4P_4)M^{II}][M^{III}(C_4P_4)M^{III}]} = \exp[(E_1° - E_2°)/25.69] \quad (3)$$

$\Delta E° = E_1° - E_2°$ in mV and at 298 K.[9] Cyclic voltammetry has been previously applied to determine the $\Delta E°$ value by estimation from $\Delta E_{1/2}$ values.[9a] From $\Delta E_{1/2}$ values, a quantitative measurement of the energetics for comproportionation reactions can be achieved. K_c values have been found to range from 4 in the uncoupled Robin and Day class I systems to 10^{13} in the strongly coupled class III systems.[10]

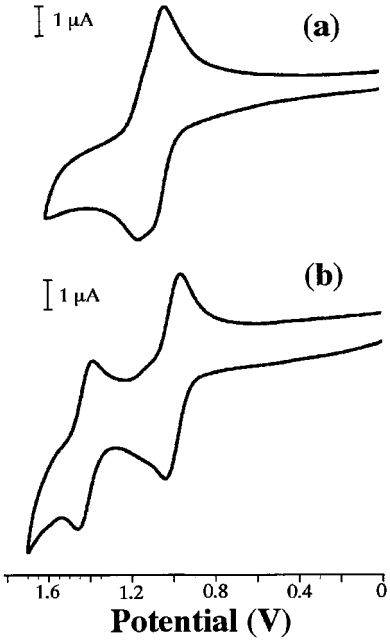

Figure 2. Cyclic voltammogram of RuC_3P_4Ru (a) and RuC_4P_4Ru (b) (0.1 M $(NBu_4)(PF_6)$ in MeCN as electrolyte; Pt disk (ca. 1 mm diameter) working electrode, Pt wire counterelectrode, and Ag/AgCl reference electrode; recorded at 22 °C).

When a molecule contains two noninteracting subunits, it is expected that the current−potential response in stationary cyclic voltammetry will be the same as that in a single-step charge transfer from a monomeric center.[9−11] The observed metal-based oxidations for MC_3P_4M correspond to two overlapping one-electron processes, indicative of a system with very weak electronic interaction (Robin and Day class I system). In contrast, for MC_4P_4M, the calculated K_c values are 1.3×10^7 (M = Ru, $\Delta E_{1/2}$ = 420 mV) and 4.5×10^{10} (M = Os, $\Delta E_{1/2}$ = 630 mV). These K_c values are comparable with those reported for species with strong electronic interaction between the two redox centers spanned by other rigid spacers such as pyrazine[9b,10,11] and phenylene.[9f] Lapinte et al.[9d,e] have also reported large redox wave separations ($\Delta E_{1/2}$ = 720 mV for the C_4 complex and 430 V for the C_8 complex) and K_c values (K_c = 1.6×10^{12} for the C_4 system and 2×10^7 for the C_8 system) for mixed-valence complexes $[Cp^*(dppe)Fe-C_n-FeCp^*(dppe)]^{n+}$, where iron centers couple directly with the C atoms in the C_n bridge. Hence, by fine-tuning the number of carbon atoms in the polyphosphine spacers, we can control the electronic interaction (or communication) between the two terminal redox centers.

In addition, from the electrochemical study we also obtained

Table 3. X-ray Photoelectron Spectroscopic Data (Binding Energies, eV) for Os(II) Complexes

sample	Os(4f)	P(2p) in PPh_2 unit	P(2p) in PF_6^- unit	N(1s)	C(1s)	F(1s)
OsC_2P_2	52.65 55.35	133.25	137.90	402.15	286.45	687.60
OsC_3P_4	52.80 55.45	133.95	138.10	402.20	286.50	687.85
OsC_4P_4	52.50 55.20	~134.0[a]	138.15	402.05	286.80	687.90
OsC_3P_4Os	52.85 55.50	133.85	138.15	402.25	286.65	687.70
OsC_4P_4Os	52.85 55.55	134.65	138.40	402.30	286.85	688.00

[a] Peak is repeatedly very weak and broad; see Figure 3.

a much greater K_c value for OsC_4P_4Os than for the corresponding RuC_4P_4Ru complex. The stronger electronic interaction displayed by the Os(II) complex here can be ascribed to the increasing M−L interaction caused by dπ−Lπ* mixing in the osmium complex (L represents the spacer). Other examples which give similar observations include the interaction between two $Ru(NH_3)_5$ units ($\Delta E_{1/2}$ = 390 mV) or two $Os(NH_3)_5$ units ($\Delta E_{1/2}$ = 760 mV) bridged by pyrazine.[10]

For the heterobimetallic complex RuC_4P_4Os, two reversible one-electron processes at +1.32 and +0.74 V are observed. These can be assigned to $Ru^{II/III}$ and $Os^{II/III}$ redox couples, respectively, on the basis of the observed redox potentials for the monometallic complexes MC_4P_4 (Table 2). Upon an anodic scan, the Os^{II} center is oxidized to Os^{III} at +0.74 V followed by the oxidation of Ru^{II} to Ru^{III} at +1.32 V, eq 4.

$$Ru^{II}(C_4P_4)Os^{II} \underset{+0.74\ V}{\overset{e^-}{\rightleftharpoons}} Ru^{II}(C_4P_4)Os^{III} \underset{+1.32\ V}{\overset{e^-}{\rightleftharpoons}} Ru^{III}(C_4P_4)Os^{III} \quad (4)$$

The ligand reduction potentials of MC_4P_4 represent two sequential one-electron reductions. The first is assigned to the $bpy^{0/-}$ redox couple ($E_{1/2}$ = −1.42 V for RuC_4P_4 and −1.32 V for OsC_4P_4, Table 2). Previously, the reported redox potential of the $bpy^{0/-}$ couple was in the range −1.27 to −1.31 V for the mono- and bimetallic Os(II) complexes with the tetratopic polyphosphine 1,2,4,5-tetrakis(diphenylphosphino)benzene.[4d] The second reduction is assigned to the second bpy $^{0/-}$ redox couple[11a] ($E_{1/2}$ = −1.67 V for RuC_4P_4 and −1.56 V for OsC_4P_4). For the bimetallic complexes MC_4P_4M (M = Ru, Os), two consecutive two-electron reductions were observed. These are also assigned to the first two $bpy^{0/-}$ redox couples (one bpy per metal center) and then the second set of $bpy^{0/-}$ redox couples.

XPS Analysis. Using X-ray photoelectron spectroscopy (XPS), we can study the electronic features of polyphosphine spacers coordinated with Ru(II) and Os(II) centers. As an important complement to the electrochemical method, XPS allows us to address the electron-donating ability of polyphosphines and the influence of carbon chain length on the electron donation.

The characteristic binding energies (in eV) of the elements involved in the series of Os(II) complexes with C_2, C_3, and C_4 chains are listed in Table 3. Among all the peaks of elements studied (including Os 4f, P 2p, N 1s, C 1s, and F 1s), *P*(2p) of the $-PPh_2$ unit is most sensitive to changes in the carbon chain length (Figure 3). This is due to the fact that the $-PPh_2$ unit binds directly to the C_n chain. An increase of 0.70−0.80 eV is observed when OsC_2P_2 is compared to OsC_3P_4 and also when OsC_3P_4Os is compared to OsC_4P_4Os. However, the signal of

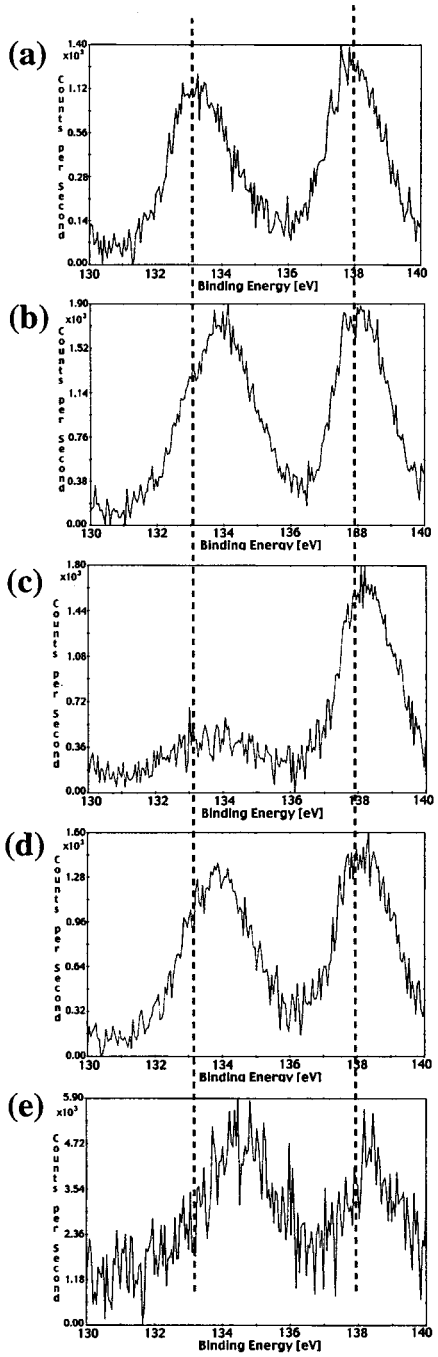

Figure 3. Comparison of XPS spectra of Os(II) monometallic and homobimetallic complexes with C_4P_4: (a) OsC_2P_2e; (b) OsC_3P_4; (c) OsC_4P_4; (d) OsC_3P_4Os; (e) OsC_4P_4Os.

P(2p, $-PPh_2$) for OsC_4P_4 is repeatedly found to be very weak and broad, with a peak position centered at ca. 134.0 eV (Table 3).

Within the P(2p) region, there is another P(2p) peak corresponding to the P atoms in the counteranion PF_6^- (Figure 3). As expected, the binding energies of these *P*(2p) peaks are less sensitive to changes in the chain length. Although we might expect to see a shift in the C(1s) peak of the C_n bridge as a function of chain length, this is thwarted by overlap of C(1s) peaks of different C atoms in the molecule.

In XPS analysis, the higher binding energy usually corresponds to less electron density on the element in question.[15] Typically, as the oxidation state increases, the binding energy of the same element increases. For example, the reported binding

Table 4. Summary of Spectroscopic Data for Complexes with C_4P_4

complex	λ_{abs}, nm (ϵ, M^{-1} cm^{-1})	λ_{em}, nm[a]	$10^{-3}\Phi$[a,b] (±10%)	τ, ns[a] (± 10%) Ru-based	τ, ns[a] (± 10%) Os-based	$\eta_{isc}k_r$,[c] s^{-1}
RuC_4P_4	285 (43 660) 450 (9 270)	540	0.05	15		3.3×10^3
OsC_4P_4	295 (43 510) 405 (8 550) 450 (8 020) 615 (2 680)	598	1.6		410	3.9×10^3
RuC_4P_4Ru	285 (94 070) 430 (19 080) 465 (20 870)	595	4.6	820		5.6×10^3
OsC_4P_4Os	290 (87 810) 410 (13 400) 450 (14 330) 610 (4 160)	660	0.20		160	1.3×10^3
RuC_4P_4Os	285 (98 960) 430 (22 780) 610 (sh, 3 030)	660	2.5	0.01	340	7.3×10^3

[a] $\lambda_{ex} = 470-480$ nm, in acetonitrile. All solution samples were treated three times with freeze−pump−thaw cycles before the measurements of emission and quantum yields. Luminescence lifetimes are obtained from the least-squares fit of single- or double-exponential decay. [b] Φ_{em} vs $Ru(bpy)_3(PF_6)_2$ ($\Phi_{em} = 0.062$). [c] $\eta_{isc}k_r = \Phi_{em}\tau^{-1}$. For RuC_4Os, τ_2 is used in the calculation. The short components in the lifetime of **3** were measured on a frequency domain fluorimeter (measurable range 50 ps−50 ns, excitation at 470 nm, monitored broad band with a cutoff filter at 500 nm). The long component of the lifetime of **3** was obtained, as were the rest of the data in this table, on a nanosecond laser system equipped with a Continuum Surelite II-10 Nd:YAG laser (lowest measurable lifetime was ca. 10 ns with a 6 ns laser pulse width; excitation at 470 nm, monitoring emission wavelength at 630 nm).

energies for P(2p) peaks of trivalent phosphines (e.g., PPh_3) are in the range 130.6−131.5 eV, while the corresponding ones of the pentavalent complexes (e.g., $(PhO)_3PO$) are higher, 133.5−134.7 eV.[15] In addition, the substituent groups on phosphine PR_3 can also play an important role in determining the binding energy. In a recent study by Benazak Holl,[16a] it was found that, upon a change of all three R groups from CH_3 to the much stronger electron-withdrawing CF_3 groups in the physisorbed PR_3 molecules on a Si surface, the $P(2p_{3/2})$ binding energy increased by 2.6 ± 0.1 eV. Hence, the neighbor groups can cause a significant shift in the binding energy of the element in question. In another study by Therien,[16b] the electron-withdrawing ability of the meso-perfluoroalkyl group on porphyrin was accessed using N(1s) core-level XPS analysis, and the N(1s) core ionization potentials were at least 0.35 and 0.1 eV larger than those of other porphyrin complexes (without perfluoroalkyl moieties) examined by this technique. For our complexes, a positive shift in the binding energy of P(2p) is observed when only the carbon chain length of the neighbor C_n groups is extended. This suggests that less electron density resides on the P atom as the carbon chain is extended.

The aforementioned electrochemical analysis shows that the redox potential of the $Os^{II/III}$ couple decreases as the carbon chain length increases, especially in the monometallic complexes. This suggests that the Os center is easier to oxidize and has more electron density when it is coordinated to the phosphine with a longer C_n chain. Upon coordination with metal centers such as Os(II), phosphines can serve as σ-donors.[17] Hence, we may conclude that the electron-withdrawing ability of the longer C_n bridge will decrease, on the basis of data from both the electrochemical study and XPS analysis. As a result, the σ-donating ability of the polyphosphine spacer appears to be enhanced and the π-acidity is weakened when the C_n chain grows. There will be less electron density on the polyphosphine (resulting in a higher P(2p) binding energy) and more electron density on the Os center (resulting in a lower redox potential for the $Os^{II/II}$ couple).

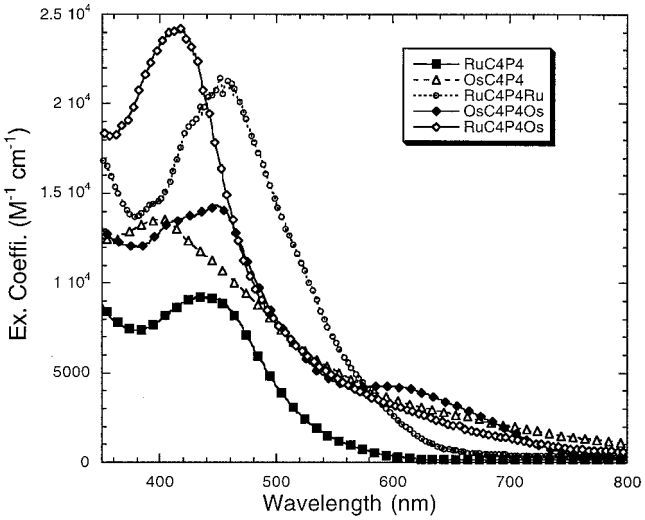

Figure 4. Electronic absorption spectra of complexes with C_4P_4 spacers (recorded in Spectrograde acetonitrile at 22 °C).

Electronic Absorption. The UV−vis absorption maxima and the corresponding extinction coefficients of the C_4P_4 complexes are listed in Table 4, and peaks in the visible region are compared in Figure 4. RuC_4P_4 exhibits a strong MLCT band (Ru → bpy) at 450 nm, and the corresponding osmium complex OsC_4P_4 exhibits a broad MLCT (Os → bpy) band at ca. 615 nm. The absorption maxima for the MLCT (M → bpy) bands for MC_4P_4M (M = Ru, Os) are observed at 465 nm for M = Ru and 610 nm for M = Os. For RuC_4P_4Os, a strong band at 430 nm (singlet MLCT in nature) is observed with a shoulder peak at ca. 610 nm (triplet MLCT in nature, tailed into 800

(15) Moulder, J. F.; Stickle, W. F.; Sobol, P. E.; Bomben, K. D.; Chastain, J. *Handbook of X-ray Photoelectron Spectroscopy*; Perkin-Elmer Corp.: 1992.
(16) (a) Zhang, K. Z.; Litz, K. E.; Banazak Holl, M. M.; McFeely, F. R. *Appl. Phys. Lett.* **1998**, *72*, 46. (b) Goll, J. G.; Moore, K. T.; Ghosh, A.; Therien, M. J. *J. Am. Chem. Soc.* **1996**, *118*, 8344.
(17) (a) Cotton, F. A.; Wilkinson, G. *Advanced Inorganic Chemistry*, 5th ed.; John Wiley & Sons: New York, 1988; Chapter 11. (b) Cotton, F. A.; Hong, B. *Prog. Inorg. Chem.* **1992**, *40*, 179.

nm). The majority of these absorption maxima are red-shifted when compared with those of the corresponding complexes[6b] with a C_3P_4 spacer and C_2P_2e. For example, when we compare the complexes OsC_2P_2e (λ_{max} = 500 nm[6b]), OsC_3P_4 (λ_{max} = 550 nm (sh)[6b]), and OsC_4P_4 (λ_{max} = 615 nm, Table 4), a significant red shift is observed. Hence, as the carbon chain length increases, the energy level of the observed ^{3}MLCT state decreases.

Steady-State and Time-Resolved Emission. Steady-state and time-resolved emission spectroscopies have been employed to study the excited-state properties including room-temperature luminescence emission and lifetime. The observed data are included in Table 4.

Regarding the monometallic complexes, the cumulene-containing complexes have emission maxima that are blue-shifted to shorter wavelengths (540 nm for RuC_4P_4 and 590 nm for OsC_4P_4) in comparison with those of $M(bpy)_3(PF_6)_2$ (620 nm[14a] and 723 nm[18a] for M = Ru and Os, respectively). This shift to a higher energy indicates that the replacement of one bpy ligand by C_4P_4 increases the energy gap between the ground state and the MLCT excited state. The same observation was also made for the vinylidene (C_2) and allene (C_3) derivatives.[6b] Such a blue shift in emission is expected when a stronger ligand (such as a polyphosphine) is used to replace a relatively weaker ligand (such as bpy).

The time-resolved emission study of OsC_4P_4 revealed a much longer luminescence lifetime (410 ns) than that of $Os(bpy)_3(PF_6)_2$ (τ = 20 ns in acetonitrile[4d,18b]). Similarly, Os(II) complexes with C_2 and C_3 also exhibit relatively long-lived ^{3}MLCT excited states with lifetimes of 190 and 350 ns for OsC_2P_2e and OsC_3P_4, respectively.[6b] This change in lifetimes can be attributed to an increase in the energy gap between ground state and the emitting ^{3}MLCT state according to the energy gap law.[4d,8] The incorporation of a stronger polyphosphine ligand will cause an increase in the energy level of the ^{3}MLCT excited state and, consequently, slow the nonradiative decay of Os(II) complexes and result in longer excited-state lifetimes. In contrast, the Ru complexes with polyphosphine spacers show much shorter lifetimes when compared with $Ru(bpy)_3(PF_6)_2$ (τ = 855 ns in acetonitrile[14a]). This observation may result from mixing of the lowest $d\pi(M)-p\pi^*(L)$ state with higher energy excited states[4d,19] and cannot be attributed solely to the change in energy gap between the ^{3}MLCT and ground states. Presumably, the mixing between the emitting ^{3}MLCT state and the dissociative nonemitting MC (ligand field) state may have an important effect here.

The homobimetallic complexes MC_4P_4M (M = Ru and Os) have red-shifted ^{3}MLCT emission maxima (λ_{em} = 595 nm for Ru and 660 nm for Os) when compared with the corresponding monomeric species MC_4P_4 (λ_{em} = 540 nm for Ru and 590 nm for Os), indicative of lower triplet energies in homobimetallic complexes. The larger difference (a shift of 70 nm) between the ^{3}MLCT emission maxima of OsC_4P_4 and OsC_4P_4Os, when compared with the corresponding Ru(II) complexes (a shift of 55 nm), can again be attributed to the increasing M−L interaction caused by $d\pi-L\pi^*$ mixing in the osmium complexes (L represents the spacer), as discussed in the aforementioned

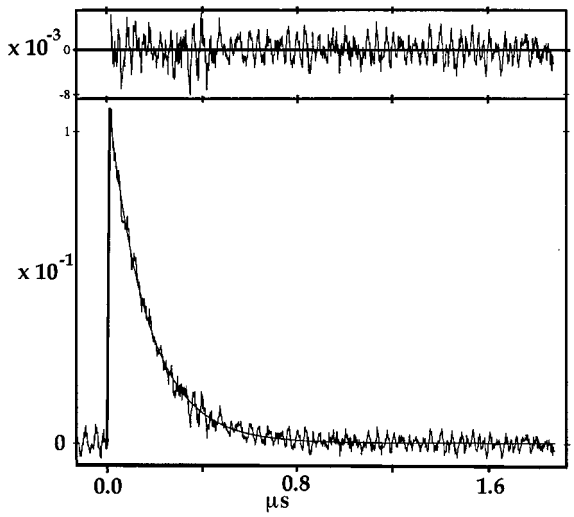

Figure 5. Excited state decay trace and fit of OsC_4P_4Os (λ_{ex} = 470 nm, λ_{em} = 660 nm; in Spectrograde acetonitrile at 295 K).

electrochemical study. Although the lifetime of RuC_4P_4Ru (820 ns) is significantly longer than that of RuC_4P_4 (15 ns), the lifetime of OsC_4P_4Os (160 ns) is decreased from that of OsC_4P_4 (410 ns). This can be explained by the fact that lowering the ^{3}MLCT excited state may have conflicting effects. While it may inhibit the mixing between the ^{3}MLCT and the higher energy metal-centered excited state, it may also enhance the mixing between the ground state and the emitting ^{3}MLCT state. In the homobimetallic Ru(II) complex the former can be dominating, while in Os(II) complex the latter may play an important role. Hence, the resulting lifetime of RuC_4P_4Ru is longer than RuC_4P_4, but the lifetime of OsC_4P_4Os is shorter than OsC_4P_4. When the intersystem crossing efficiency (to populate the MLCT triplet state), η_{isc}, is included, the radiative decay rate constant, k_r, can be expressed as $k_r = \Phi_{em}/\eta_{isc}\tau$ or $\eta_{isc}k_r = \Phi_{em}/\tau$.[14] The values are found to be ca. $(1.3-7.3) \times 10^3$ s^{-1} for all the complexes with C_4P_4 (Table 4). These values are consistent with the data observed for complexes with the C_3P_4 spacer (ca. 2.8×10^3 to 1.7×10^4 s^{-1}) but lower than those observed (ca. 1.6×10^4 to 1.6×10^5) for complexes with C_2P_2e.[6b] The lower observed radiative decay constants may imply either rapid relaxation of the ^{1}MLCT state back to the ground state before a substantial amount of intersystem crossing can occur or the formation of another lower energy state, or a combination of both.

Transient Absorption. Figure 6 gives the comparison of the differential absorption spectra of monometallic (Figure 6a) and homobimetallic (Figure 6b) complexes with C_2P_2e, C_3P_4, and C_4P_4. The spectra were recorded at 150 ns after the laser pulse (pulse width 6 ns) upon excitation at 510−520 nm. Each spectrum has a characteristic absorption peak at 375 nm, corresponding to the absorbing $\pi \rightarrow \pi^*$ band of the coordinated bipyridine. Bleaching of the MLCT absorption bands in the region 400−550 nm is observed. An additional weak absorption at 450−510 nm is also found in the spectra of OsC_2P_2e and OsC_3P_4, which can be ascribed to the weakly absorbing charge-transfer band. In addition to that of RuC_4P_4Ru, attempts have been made to obtain the transient absorption spectra of other mono- and bimetallic complexes with Ru(II) centers. However, no significant signal was observed.

Molecular Modeling and Metal-to-Metal Distance. Molecular modeling studies were performed using the MSI InsightII program (ESFF force field, v. 97.0, Molecular Simulations, Inc.) to obtain the metal-to-metal distances in the heterobimetallic

(18) (a) Creutz, C.; Chou, M.; Netzel, L.; Okumura, M.; Sutin, N. *J. Am. Chem. Soc.* **1980**, *102*, 1309. (b) Barigelletti, F.; Juris, A.; Balzani, V.; Belser, P.; von Zelewsky, A. *Inorg. Chem.* **1983**, *22*, 3335.

(19) (a) Juris, A.; Belser, P.; Barigelletti, F.; von Zelewsky, A.; Balzani, V. *Inorg. Chem.* **1986**, *25*, 256. (b) Winkler, J. R.; Netzel, T. L.; Creutz, C.; Sutin, N. *J. Am. Chem. Soc.* **1987**, *109*, 2381. (c) Fuchs, Y.; Lofters, S.; Dieter, T.; Shi, W.; Morgan, R.; Strekas, T. C.; Gafney, H. D.; Baker, A. D. *J. Am. Chem. Soc.* **1987**, *109*, 2691.

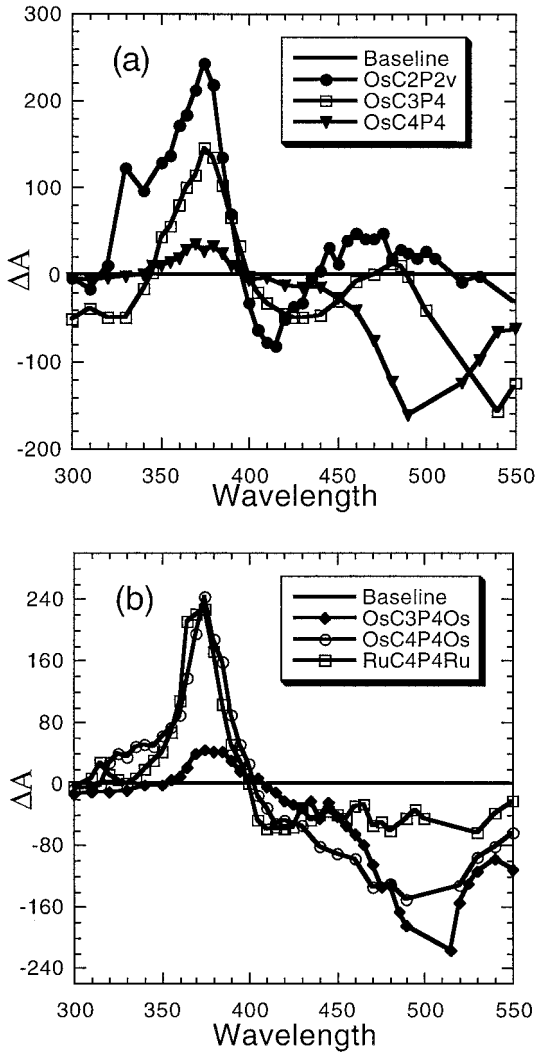

Figure 6. Transient absorption spectra of Os(II) complexes (recorded in Spectrograde MeCN at 22 °C). Excitation wavelengths are 500−520 nm, and data presented are 150 ns after the initial laser pulse (pulse width 6 ns). $\lambda_{ex} = 520$ nm for OsC_2P_2e, OsC_3P_4, and RuC_4P_4Ru; $\lambda_{ex} =$ 510 m for OsC_4P_4, OsC_3P_4Os, and OsC_4P_4Os.

complexes. Figure 7 gives the stick-and-ball structures for the rigid molecules with C_3 and C_4 bridges. The metal-to-metal distances thus measured are 8.66 Å for RuC_3P_4Os and 9.87 Å for RuC_4P_4Os. Although diastereoisomeric forms[21] may exist in the current system, such distances were obtained after the structural optimization and the minimization of steric repulsion.

Intervalence Charge Transfer (IVCT) and Near-IR Study. Chemical oxidation of one Os(II) center to Os(III) in mixed-metal (Ru^{II}/Os^{II}) and homobimetallic complexes will generate mixed-valence complexes and allow the spectroscopic measurement of the oxidized species. Typically, the appearance of a characteristic intervalence charge transfer (IVCT) band in the visible and near-IR regions is useful in evaluating the electronic coupling and delocalization across different spacers. The energies and intensities of these absorption bands have been used to classify mixed-valence complexes according to the degree

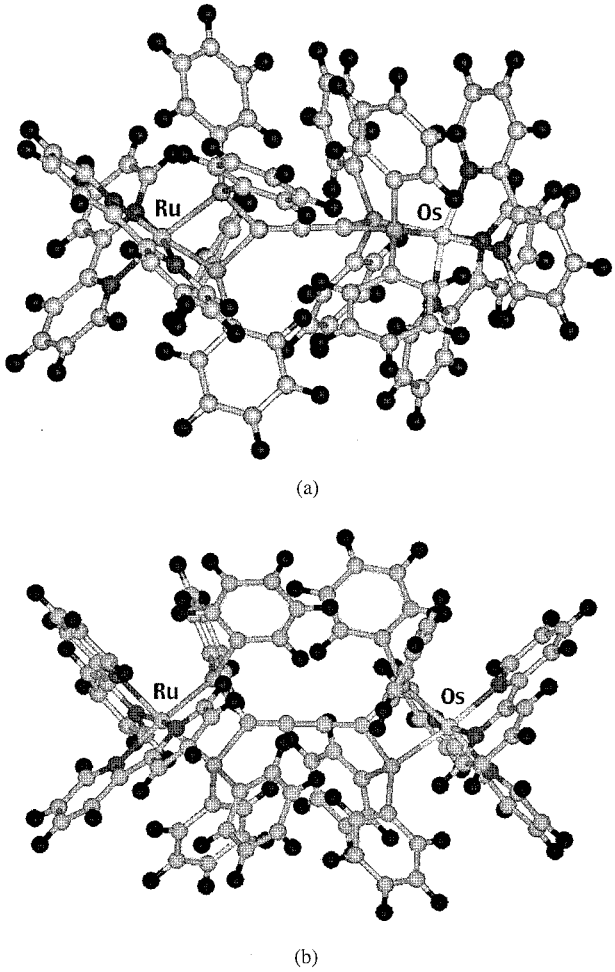

Figure 7. Molecular modeling of RuC_3P_4Os (a) and RuC_4P_4Os (b).

of delocalization across the spacers.[5,20] Class I mixed-valence complexes (completely localized) rarely have IVCT transitions, while class III complexes (highly delocalized) may have narrow and intense absorption bands in the visible and near-IR regions. Class II (partially delocalized) complexes may also display characteristic IVCT bands in the visible and near-IR regions. Hence, the study of the IVCT band, in addition to the evaluation of the comproportionation constant K_c, will allow us to characterize the electronic interaction across rigid polyphosphine spacers with allene and cumulene.

Upon oxidation with $(NH_4)_2Ce(NO_3)_6$ in a 10:1 MeCN−H_2O mixture solvent, the oxidized mixed-metal compound $Ru^{II}C_4P_4Os^{III}$ gives an intervalence transition at 1050 nm (9524 cm^{-1}, $\epsilon = 75\ M^{-1}\ cm^{-1}$) with a bandwidth of $\Delta\nu_{1/2} = 825\ cm^{-1}$ (Figure 8). No band was observed in this region for the unoxidized $Ru^{II}C_4P_4Os^{II}$ complex. However, a near-IR study performed on the FT-IR spectrometer (Bruker model IFS 66) reveals no significant IVCT band in the scanned region (7000−12 000 cm^{-1}) for RuC_3P_4Os and OsC_nP_4Os ($n = 3$, 4) upon oxidation of one Os(II) center with Ce^{4+}.

The magnitude of the electronic interaction between the two metal centers in the mixed-valence species is often expressed in terms of a coupling parameter, H_{AB} (in cm^{-1}), as explained by Hush and Creutz.[20] The magnitude of H_{AB} can be estimated using eq 5,[5,20a,b] where ϵ is the extinction coefficient of the IVCT

$$H_{AB} = \frac{2.05 \times 10^{-2}(\epsilon\, \Delta\nu_{1/2}\, E_{op})^{1/2}}{r} \qquad (5)$$

(20) (a) Creutz, C. *Prog. Inorg. Chem.* **1983**, *30*, 1. (b) Hush, N. S. *Prog. Inorg. Chem.* **1967**, *8*, 391. (c) Sutin, N. *Acc. Chem. Res.* **1982**, *15*, 275.

(21) (a) Keene, F. R. *Chem. Soc. Rev.* **1998**, *27*, 185−193. (b) Kelso, L. S.; Reitsma, D. A.; Keene, F. R. *Inorg. Chem.* **1996**, *35*, 5144. (c) Rutherford, T. J.; Van Gijte, O.; Mesmaeker, A. K.-D.; Keene, F. R. *Inorg. Chem.* **1997**, *36*, 4465.

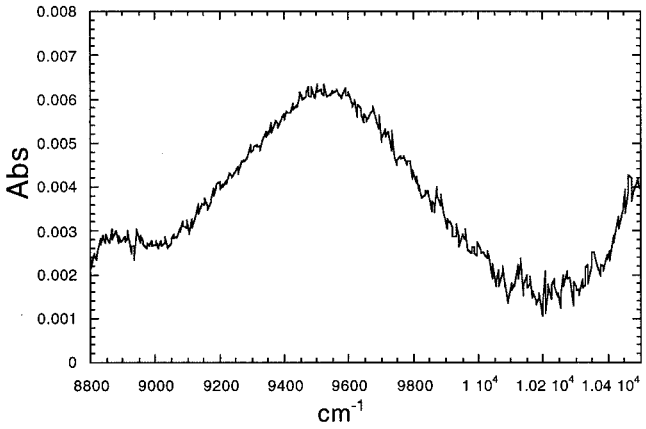

Figure 8. Near-IR spectrum of the mixed-valence complex $Ru^{II}C_4P_4Os^{III}$ (in Spectrograde acetonitrile at 295 K).

band in M^{-1} cm^{-1}, $\Delta\nu_{1/2}$ is the bandwidth at half-height of the IVCT band in cm^{-1}, E_{op} is the energy of the IVCT transition maximum in cm^{-1}, and r, according to the simplest interpretion,[5c,22b] is the geometric distance between the metal ions in Å. When the value of r is estimated as the metal-to-metal distance (9.87 Å), the calculated value for H_{AB} of RuC_4P_4Os is ca. 49 cm^{-1}. One may object that the metal-to-metal distance is probably a structural parameter not fully appropriate for the calculations discussed here, since the MLCT states may involve, to some extent, the auxiliary bpy and perhaps also the C_4P_4 spacer.[22b] Although it is reasonable to assume that the calculated H_{AB} value is in the range of those for a class II system,[9,10,22] we cannot completely exclude the possibility that the observed IVCT band might correspond to a low-intensity, high-energy class III transition because of two reasons: (a) the observed $\Delta\nu_{1/2}$ (825 cm^{-1}) is very narrow when compared with the IVCT transitions in other class II type complexes[5,20] and (b) very large values of the comproportionation constant ($K_c = 1.3 \times 10^7$ for M = Ru and 4.5×10^{10} for M = Os) have been observed for the corresponding complexes MC_4P_4M (M = Ru, Os).

In addition to the study of mixed-valence Ru/Os complexes using chemical oxidation with Ce(IV), reflectance near-IR spectroelectrochemistry (NIR SEC) was used to observe and measure the IVCT band of the induced mixed-valence states of the Ru/Os complexes with C_3 or C_4 bridges. For RuC_4P_4Os, the $Os^{II/III}$ redox couple occurs at 0.74 V while $Ru^{II/III}$ occurs at 1.32 V. Therefore, at a voltage between the two redox couples (0.74−1.32 V), the Os center should be in the oxidized form while the Ru center remains in an unoxidized state. At a solution voltage of 1.215 V, a signal was observed at 1025 nm (9756 cm^{-1}, $\epsilon = 90$ M^{-1} cm^{-1}) with a bandwidth of $\Delta\nu_{1/2} = 1250$ cm^{-1}. This result, though slightly different, corresponds with that observed in the chemical oxidation experiments (1050 nm). Using eq 5, the magnitude of H_{AB} was calculated to be ca. 69 cm^{-1}. Hence, the degree of electronic interaction between the two metals was found to be slightly higher when the mixed-valence state was reached electrochemically but remained very close to that obtained by the chemical oxidation using $(NH_4)_2Ce(NO_3)_6$. Attempts were also made to access the IVCT bands, if any, for the complexes RuC_3P_4Os and OsC_4P_4Os using photoelectrochemical methods. However, no significant peak was observed.

From the aforementioned study of cyclic voltammetry and redox interaction, we have learned that the conjugated C_4 bridge will facilitate the electronic interaction across the spacer, while the allene bridge with 90° rotation of the two sets of pπ orbitals at the central carbon atom will minimize the redox communication. This is supported by the observation in the IVCT band study. The fact that no IVCT band is observed for RuC_3P_4Os confirms its assignment as a class I complex, while the appearance of the IVCT band at 1025−1050 nm suggests a better metal−metal interaction between two termini spanned by C_4P_4.

Energy Transfer. Upon excitation at 470 nm in acetonitrile, where the Ru(II) chromophore absorbs approximately 62% of the incident photons on the basis of a comparison of extinction coefficients for RuC_4P_4Ru and OsC_4P_4Os, an emission at 660 nm is observed from RuC_4P_4Os. Excitation at 600 nm, where the Os(II) component is the dominant chromophore, results in the appearance of the same Os(II) ^{3}MLCT emission at 660 nm. This suggests an efficient energy transfer from Ru(II) to Os(II) upon excitation at 470 nm. The free energy change $\Delta G°$ for energy transfer can be expressed as the difference between the spectroscopic energies of the energy donor (Ru^{II}-based) and acceptor (Os^{II}-based), by following the conventional assumptions.[3,20c,22] The actual calculated value is ca. 1655 cm^{-1} (0.21 eV), estimated from the energy of emission maxima for homobimetallic complexes with C_4P_4.

The energy transfer rate constant (k_{en}) can be estimated using eq 6,[22] where τ_m and τ represent the luminescence lifetimes of

$$k_{en} = 1/\tau - 1/\tau_m \qquad (6)$$

the suitable model complex and the actual heterobimetallic complex. RuC_4P_4Ru is used here as the model complex for the donor, and a single-exponential decay is observed with τ_m = 820 ns upon excitation at 470 nm. For RuC_4P_4Os, a longer lifetime component is observed with τ = 340 ns, which is assigned to the Os(II) ^{3}MLCT emssion. In addition, a very short-lived component of ca. 0.01 ns is also detected. Presumably, this short component corresponds to the quenched Ru(II) ^{3}MLCT excited state as a result of intercomponent energy transfer. Hence, the rate constant for energy transfer across a rigid C_4P_4 spacer can be estimated as ca. 1.0×10^{11} s^{-1}. When compared with the observed k_{en} of the corresponding RuC_3P_4Os complex with allene, which has a maximum value of 3.0×10^9 s^{-1},[6b] the current energy transfer rate constant is significantly higher. This suggests that C_4P_4 is a much better spacer in mediating electronic energy transfer, despite the fact that it has longer length than C_3P_4. Presumably, the increased electronic interaction between the metal centers spanned by C_4P_4 facilitates the energy transfer from the Ru^{II}-based donor to the Os^{II}-based acceptor.

The mechanism by which energy transfer occurs in systems containing Ru(II)− and Os(II)−polypyridyl units linked by flexible (e.g., alkanes[23]) or rigid organic spacers (e.g., polyphenylene[22]) has been interpreted as either a Förster-type or a Dexter-type mechanism, or both. For systems containing C_3P_4, a Dexter meachanism has been proposed.[6b] The mechanism of energy transfer across C_4P_4 will be discussed here.

(22) (a) Barigelletti, F.; Flamigni, L.; Balzani, V.; Collin, J.-P.; Sauvage, J.-P.; Sour, A.; Constable, E. C.; Thompson, A. M. W. C. *J. Am. Chem. Soc.* **1994**, *116*, 7692. (b) Schlicke, B.; Belser, P.; De Cola, L.; Sabbioni, E.; Balzani, V. *J. Am. Chem. Soc.* **1999**, *121*, 4207.

(23) (a) Ryu, C. K.; Schmehl, R. H. *J. Phys. Chem.* **1989**, *93*, 7961. (b) De Cola, L.; Balzani, V.; Barigelletti, F.; Flamigni, L.; Belser, P.; von Zelewsky, A.; Frank, M.; Vögtle, F. *Inorg. Chem.* **1993**, *32*, 5228. (c) Furue, M.; Yoshidzumi, T.; Kinoshita, S.; Kushida, T.; Nozakura, S.; Kamachi, M. *Bull. Chem. Soc. Jpn.* **1991**, *64*, 1632. (d) Schmehl, R. H.; Auerbach, R. A.; Walcholtz, W. F. *J. Phys. Chem.* **1988**, *92*, 6202. (e) Schmehl, R. H.; Auerbach, R. A.; Walcholtz, W. F.; Elliott, C. M. *Inorg. Chem.* **1986**, *25*, 2440.

For energy transfer via a Förster-type dipole−dipole (through-space) mechanism, the appropriate spectroscopic overlap integral (J_F) can be expressed as eq 7,[7] where $F(\upsilon)$ is the luminescence

$$J_F = \frac{\int F(\nu)\,\epsilon(\nu)\,\nu^{-4}\,d\nu}{\int F(\nu)\,d\nu} \quad (7)$$

intensity at wavelength υ (in cm^{-1}) and $\epsilon(\upsilon)$ is the molar extinction coefficient (in $M^{-1}\ cm^{-1}$). The J_F value thus calculated is $7.1 \times 10^{-14}\ cm^6\ mol^{-1}$ (±10%) for the heterobimetallic complex RuC_4P_4Os. The derived value here is of magnitude comparable to those of the estimated overlap integrals previously reported for systems with rigid alkyne-[7a] or phenylene-bridged[22] Ru/Os complexes. The rate constant for triplet energy transfer occurring by the Förster mechanism can then be calculated using eq 8,[7b,c] where K is the orientation factor

$$k_F = \frac{8.8 \times 10^{-25} K^2 \Phi_L J_F}{n^4 \tau_L R^6} \quad (8)$$

relating to the alignment of transition dipoles on donor and acceptor ($K^2 = 0.67$[7b]), Φ_L and τ_L are the quantum yield and excited-state lifetime of the appropriate model complex RuC_4P_4-Ru, and n is the refractive index of the solvent acetonitrile. At 295 K, the calculated k_F value is $(8 \pm 1) \times 10^7\ s^{-1}$ over a metal-to-metal distance of $r = 9.87$ Å. This calculated Förster energy transfer rate constant is much lower than the observed value of ca. $1.0 \times 10^{11}\ s^{-1}$ for RuC_4P_4Os. Hence, the Förster mechanism is not suitable here.

The rate constant of the Dexter-type energy transfer can be expressed in the nonadiabatic limit as in eq 9.[3,22] The electronic

$$k_D = \nu_{en} \exp(-\Delta G^{\ddagger}/RT) \quad (9)$$

frequency ν and the free activation energy $\Delta G^{\ddagger}$ can be evaluated according to eqs 10 and 11,[22] where ΔG° is the difference

$$\nu = (2H^2/h)(\pi^3/\lambda RT)^{1/2} \quad (10)$$

$$\Delta G^{\ddagger} = (\lambda/4)(\lambda + \Delta G^{\circ}/\lambda)^2 \quad (11)$$

between the spectroscopic energies of donor and acceptor (ca. 1655 cm^{-1} or 0.21 eV). The reorganization energy λ can be estimated from the Stokes shift[22] of the acceptor (ca. 1240 cm^{-1} or 0.15 eV). The calculated value of $\exp(-\Delta G^{\ddagger}/RT)$ is approximately 1 and, hence, k_D is almost equal to ν. From eq 10, ν_{en} is estimated as $[(5.65 \times 10^8)H^2]\ cm^{-2}$. To obtain an energy transfer rate constant that is $10^{11}\ s^{-1}$, only an electronic interaction energy H of ca. 13 cm^{-1} is needed by the assumption of an exchange mechanism. Efficient electronic communication across the C_4P_4 spacer has been revealed by the cyclic voltammetry study, and the aforementioned study of the IVCT band has also given the coupling parameter H_{AB} a value of ca. 49 cm^{-1}. Hence, we may conclude that the electronic energy transfer is taking place via a Dexter-type mechanism in RuC_4P_4Os.

Conclusions

We have shown that rigid spacers with cumulenic (C_n) sp carbon chains are suitable novel types of molecular building blocks in the construction of molecular rods. Mono-, homo-, and heterobimetallic compounds containing this type of spacer exhibit interesting electrochemical and photophysical properties as well as tunable electronic communication between the terminal sites upon a change in the carbon chain length. Specifically, in the electrochemical study, it is observed that the length of C_n bridges has a profound influence on redox potentials and the electronic interaction between the two metal-based termini. XPS results reveal that a simple change in carbon chain length will affect electron donation of the spacer to the metal-based termini. As a result, the redox potential of Ru(II) or Os(II) and the P(2p) binding energies in the $-PPh_2$ units of spacers shift significantly. From the cyclic voltammetry study, the comproportionation constant K_c is calculated as 1.3×10^7 ($M = Ru^{II}$) or 4.5×10^{10} ($M = Os^{II}$) for MC_4P_4M (M = Ru, Os), suggesting a strong electronic communication across C_4P_4. However, the K_c values are estimated to be ca. 4 for the corresponding complexes MC_3P_4M (M = Ru, Os), indicative of a system with electronic isolation between two redox-active termini. In the heterobimetallic Ru(II)/Os(II) systems MC_nP_4M ($n = 3, 4$), the energy transfer from Ru(II)- to the Os(II)-based moiety is found to be very efficient, with rate constants k_{en} of ca. $3 \times 10^9\ s^{-1}$ ($n = 3$) and $1 \times 10^{11}\ s^{-1}$ ($n = 4$). The increased value of k_{en} upon the increase in chain length from C_3 to C_4 can be explained by the change in electronic communication. From the available data and calculations, a Dexter-type of mechanism can be proposed to account for the efficient triplet energy transfer across C_n-bridged polyphosphines.

Acknowledgment. This work was supported by the University of California, Irvine, and by a National Science Foundation CAREER award (CHE-9733546). We thank Prof. Wayne E. Jones and his graduate student Clifford Murphy (State University of New York at Binghamton) for the measurement of the lifetime of RuC_4P_4Os on a frequency domain fluorimeter. We thank Dr. Wytze van der Veer (UCI laser facility) and Dr. John Greaves (UCI mass spectral laboratory) for their assistance in the time-resolved emission study and FAB/MS and MALDI-TOF/MS analysis. We also thank Prof. V. Ara Apkarian for the use of the Bruker IFS-66 FT-IR spectrometer.

IC990673M